Modeling and evaluation of freeform extruded filament based on numerical simulation method for direct ink writing

Yongqiang Tu, Alaa Hassan, Javier Arrieta-Escobar, Uzair Khaleeq Uz Zaman, Ali Siadat, Gongliu Yang

Modeling and evaluation of freeform extruded filament based on numerical simulation method for direct ink writing

Yongqiang Tu[a,b], Alaa Hassan[c,*], Javier A. Arrieta-Escobar[c], Uzair Khaleeq uz Zaman[d], Ali Siadat[b], Gongliu Yang[a]

(*Corresponding author: Alaa Hassan; Email address: alaa.hassan@univ-lorraine.fr)

[a]School of Instrumentation and Optoelectronic Engineering, Beihang University, Beijing 100191, PR China

[b]Université de Lorraine, Arts et Métiers ParisTech, LCFC, F-57000 Metz, France

[c]Université de Lorraine, ERPI, F-54000 Nancy, France

[d]Department of Mechatronics Engineering, National University of Sciences and Technology, Islamabad, Pakistan

Abstract

Direct ink writing (DIW) is an extrusion-based additive manufacturing (AM) technique. One of the required factors for printing quality in DIW is to extrude continuous and tubular freeform extruded filaments (FEF) with diameters close to the nozzle inner diameter. This paper established a simulation model of FEF with volume of fluid (VOF) method and then evaluated the FEF based on the simulation results. First, ink properties including density, surface tension coefficient and rheological properties were determined by properties tests. Then, the model of FEF was established using VOF simulation method with the software OpenFOAM and two evaluation indicators, mean diameter and stability, were proposed to evaluate the FEF. Two inks, a cellulose ink and a Nivea Crème, were used under three levels of piston velocity to verify the method universality for different inks and variable process parameters. The prediction accuracy of the established simulation model was verified as the relative error between simulation and experimental results of diameter was less than 10.22%. In this work, it was found that: (1) piston velocity needed to be set higher than a minimum value to overcome yield stress and surface tension to successfully extrude filaments; (2) mean diameter of FEF decreased while stability of FEF decreased firstly and then increased as piston velocity increased. The proposed model and evaluation indicators gave an accurate and effective framework to analyze effect of the piston velocity on FEF, characterize the ink printability and find suitable printable windows for process parameters in DIW.

Keywords

Modeling; evaluation; numerical simulation; freeform extruded filament; direct ink writing

Statements and Declarations

Authors contributions

YT: Methodology, Writing- original draft. AH: Conceptualization, Methodology, Writing –review & editing. JA: Test, Writing- original draft. UKZ: Writing –review & editing. AS: Supervision. GY: Supervision.

Funding

This work has been supported by the China Scholarship Council (No. 201906020135).

Data availability

The authors confirm that all data and materials reported in this paper are available.

Conflict of interest

On behalf of all authors, the corresponding author states that there is no conflict of interest.

Ethical approval

Not applicable.

Consent to participate

Not applicable.

Consent to publish

Not applicable.

1. Introduction

Direct ink writing (DIW), which was firstly proposed by Cesarano et al. in 1998 [1] and was patented in 2000 [2], is an extrusion-based additive manufacturing (AM) technique by depositing slurry or paste type materials named inks onto the substrate layer by layer [3]. Compared with other AM techniques, DIW has advantages in materials flexibility, low cost and reliability [4]. Due to the advantages, various materials have been made into inks suitable for DIW and been successfully used in various applications: polymer inks for rubber industry[5]; bio-inks with living cells for tissue engineering and regenerative medicine [6]; metal inks for batteries and electronic circuits [7]; ceramic inks for ceramic engineering [8]; cellulose inks for clothing, sensors and 4D printing [9-11]; food inks for food processing engineering [12]; cement ink for buildings [13]. In the foreseeable future, more materials will be prepared into inks suitable for DIW and used in more fields. Thus, DIW is a research focus in AM studies and regarded as an important technique to realize advanced and intelligent manufacturing nowadays [14].

Freeform extruded filaments (FEF) were extruded filaments in the air between the nozzle bottom and the substrate in DIW. During the DIW, producing continuous, tubular FEF with diameters close to the actual nozzle inner diameter is a prerequisite and also a characterization for a high printing quality [15]. For instance, Ouyang et al. [16] characterized ink printability through shape statuses of FEF; Paxton et al. [17] focused on the formation properties of FEF as an initial screening to assess ink printability; Smith et al. [15] proposed a term considering the measured diameter of the FEF and nozzle inner diameter to define printability; Dávila et al. [18] evaluated ink printability through observation of FEF formation; He et al. [19] chose suitable ranges for process parameters setting in DIW 3D printers by observing shapes of FEF. Therefore, modeling and evaluation of FEF are necessary for quality evaluation and control for DIW.

Recently, filaments in extrusion-based AM have been modeled and evaluated mainly through analytical methods [20], experimental methods [21] and numerical simulation methods [22]. Analytical methods give a model based on the mathematical description and derivation of physical process, but model accuracy is restricted by theoretical simplification. Experimental method presents a regression model between input factors and experimental results, but this method is restricted by measurement method and cannot provide a dynamic prediction. In complement to analytical and experimental methods, numerical simulation methods can deliver a vast amount of information about the process and has proven to be an accurate and reliable dynamic predictive tool in the analysis of extrusion-based AM techniques [23-25].

However, there is few works on modeling and evaluation of FEF based on numerical simulation methods for DIW. Numerical simulation modeling of FEF should fully consider ink's properties and process parameters as the quality of FEF depends both on ink's material properties and process parameters setting [26]. Evaluation of FEF should consider both the mean diameter and the stability as these two indicators have the most significant influence on the printing quality [27].

The aim of this study is to establish a model of FEF with numerical simulation method and then evaluate the FEF based on this model. First, ink properties including density, surface tension coefficient and rheological properties were determined by properties tests. Then,

model of FEF was established using numerical simulation method and two evaluation indicators, mean diameter and stability, were proposed to evaluate the FEF. Finally, two inks, the cellulose ink and Nivea Crème, were used under three levels of piston velocity to verify the method. After experimental verification, the model and evaluation indicators were used to analyze effect of the piston velocity on FEF, characterize the ink printability and find suitable printable windows for process parameters.

2. Ink preparation and properties tests

2.1. Ink preparation

To verify the proposed method considering the universality for different materials, two well printable inks, the cellulose ink with low viscosity and Nivea Crème with high viscosity, were prepared.

Cellulose inks, which mainly contain cellulose fibers and cellulose derivatives, are representatives of novel inks for DIW [28, 29]. The cellulose ink used was prepared by mixing 2.36% natural cellulose fibers, 0.59% hydroxyethyl cellulose (HEC), 1.77% carboxymethyl cellulose (CMC), 0.47% montmorillonite, 0.47% citric acid (CA) and 94.34% demineralized water [9]. Cotton linter packs (CLP) (Goetz & Sons, Inc., USA) were purchased as natural cellulose fibers. CLP were first left in demineralized water for 24 hours and then dried at room temperature (25 °C). Once dried, CLP were added to a beaker with demineralized water and the montmorillonite (reference: 42531) and mixed with a spatula. HEC (reference: 54290) and CMC (reference: Acros Organics 332641000) were mixed and then added to the mixture in the beaker. One quarter of the polymer mixture was added into the beaker and mixed for 1 min at 700 rpm by planetary mill with 5 grinding balls of zirconium oxide (Ø20 mm) using a Pulverisette 7 Premium Line (Fritsch, Germany). The remaining polymer mixture was then incorporated, followed by another grinding cycle under the same conditions. CA (reference: C0759) was added to the combination of all batches prepared as a crosslinking agent on the same day by means of a spatula.

Nivea Crème with well printability is often used as printability reference for inks to test the process parameters in DIW [17] as many inks in DIW are designed and produced to have the same printability of Nivea Crème [30]. In this study, Nivea Crème (Art. No. 80104) (Beiersdorf Global AG, Germany) with high viscosity and well printability was chosen and bought.

2.2. Ink material properties tests

A 5 mL pycnometer and analytical balance XSR (both from Mettler Toledo, France) were used to assess ink density by measuring a mass of 5 mL of the ink (measuring accuracy: 0.008 mg). A tensiometer K9 (KRÜSS, Germany) was used to measure the surface tension coefficient using the Du Noüy ring method (measuring accuracy: 0.1 mN/m). For both tests, measurements were performed at 25 ℃.

The Hershel-Bulkley model (HBM) has been verified and adopted as a suitable and reliable model to represent the viscosity of the shear thinning inks in DIW [31, 32]. Using the HBM, the shear stress and the viscosity of inks can be expressed by Eq. (1) and Eq. (2), respectively.

$$\tau = \tau_0 + K\dot{\gamma}^{\cdot} \quad . \tag{1}$$

$$\mu=\min\left(\mu_0,\tau_0/\dot{\gamma}\right) \quad (2)$$

Where τ (unit: Pa), $\dot{\gamma}$ (unit: s^{-1}), μ (unit: $Pa\cdot s$) are variables named as shear stress, shear rate, dynamic viscosity for inks in flow; μ_0 (unit: $Pa\cdot s$), τ_0 (unit: Pa), K (unit: $Pa\cdot s^n$), n (unit: dimensionless) are rheological properties called as limiting dynamic viscosity, yield stress, consistency index, flow index for inks. If stress< τ_0, the ink behaves as a rigid solid, otherwise it behaves as a fluid. For n <1, the ink is shear-thinning, whereas the ink is shear-thickening. A large μ_0 means that the ink will only flow in response to a large applied force. A rheometer ARES (TA Instruments, USA) with a 25 mm plate-plate geometry at a gap distance of 1 mm was used to obtain parameters in Eq. (1) and Eq. (2). μ_0, τ_0 were determined by shear stress ramp test ranging from 0.01 to 100 Pa: abscissa and ordinate of intersection point between two linear regressions at the plateau-region and viscosity-drop regions of the viscosity-shear stress diagrams was μ_0 and τ_0, respectively. K, n were determined by shear rate sweep test ranging from 0.0125 to 1000 s^{-1} (5 points per decade) through regression between Eq. (2) and experimental viscosity-shear rate data.

3. Modeling and evaluation indicators

3.1. Meshes and boundary conditions

The numerical simulation was implemented within the software OpenFOAM, which is a free, open-source and popular numerical simulation software for computational fluid dynamics (CFD) simulations [33]. In the modeling, OpenFOAM was used to build geometrical model, generate meshes, determine boundary conditions and solve governing equations. ParaView, an open-source, multi-platform data analysis and visualization application, was used to build visualizations and analyze data obtained by OpenFOAM.

As shown in Fig. 1a, FEF was produced by extruding ink in the syringe through the nozzle into the air with the piston movement. Dimensions of the geometrical model of FEF in DIW include: the inner diameter of syringe D_s; the ink filled length L_s; the nozzle inner diameter D_n; the nozzle length L_n; the gap between nozzle bottom and substrate h. In this study, h was set as 26 mm to avoid FEF touching the substrate. D_s, D_n, L_n and the initial L_s were set to match the actual device dimensions: 21.6 mm, 0.84 mm, 18 mm, 30 mm, respectively. Fig. 1b presents the 3D model established in OpenFOAM for FEF at the initial time, where red regime represents the ink and blue regime represents the air. As shown in Fig. 1c, the 3D model was simplified into a 2D axisymmetric model by capturing 1/120 of the 3D model in the circumferential direction to reduce computation cost under the axisymmetric laminar flow condition for the ink extrusion.

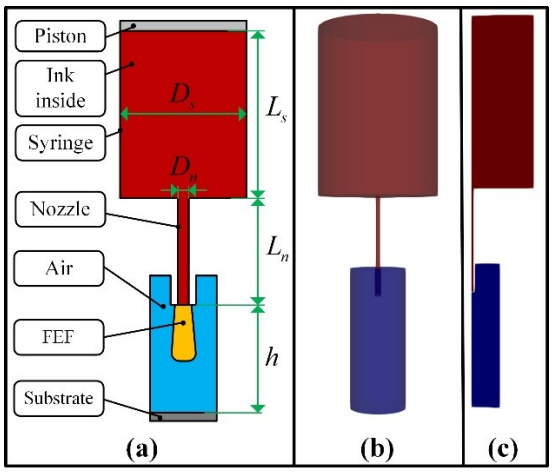

Fig. 1 Geometrical model of FEF in numerical simulation for DIW: (a) dimensions of the geometrical model; (b) established 3D model at the initial time; (c) simplified 2D axisymmetric model at the initial time.

OpenFOAM is designed as a code for 3D space and defines all meshes as 3D meshes, but wedge type meshes are used for 2D axisymmetric problems specifically [34]. Thus, wedge type meshes were used for the simplified 2D axisymmetric model as shown in Fig. 2a, where lengths and widths of meshes in the same area were set nearly same and meshes in the junction of different areas were refined to improve calculation accuracy. Total number of the meshes was 18996. Boundary conditions were grouped into 5 categories and were defined as shown in Fig. 2b and Table 1.

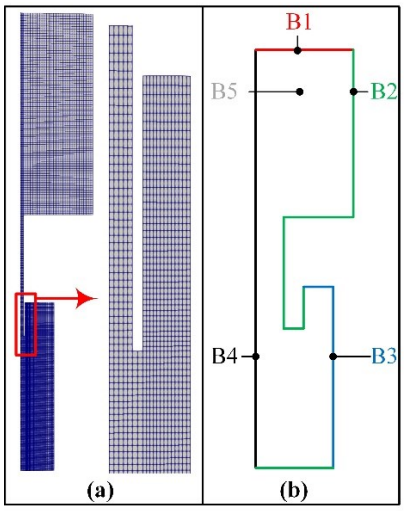

Fig. 2 Meshes and boundary conditions for model of FEF in numerical simulation for DIW: (a) meshes; (b) boundary conditions.

Table 1 Definition of boundary conditions

Name	Physical meaning	Type	Setting
B1	Piston	Moving boundary	Velocity is equal to piston velocity
B2	Inner walls of syringe; walls of nozzle and substrate	No-slip boundary	No-slip
B3	Air	InletOutlet boundary	Depended on dynamic calculation
B4	Symmetrical axis	Symmetrical boundary	Empty condition

B5	Front and back side symmetrical sections	Wedge boundary	Symmetrical condition

3.2. Volume of fluid method

The volume of fluid (VOF) method [35] was chosen to capture the interface of FEF in the air. Compared with other CFD numerical simulation methods like level set method [36], phase field method [37], lattice-Boltzmann method [38] and direct interface tracking method [39], VOF method has been proven to be a priority choice for the simulation of two-phase flows due to its simplicity, robustness and straightforward implementation and been widely used in numerical simulation for extrusion-based AM [25].

In VOF method, the ink and the air were treated as a single continuum and the phase fraction α was defined to distinguish the interface between the two-phase fluid as follows:

$$\alpha = \frac{V_i}{V_m}. \tag{3}$$

Where α is the phase fraction for a mesh; V_i is the volume of the ink in the mesh; V_m is the total volume of the mesh. Values of α are between 0 to 1 and α =0.5 is defined as the cutoff value to capture the sharp front of interface between the ink and the air.

Fluid properties of the single continuum were weighted with the phase fraction as follows:

$$\begin{aligned} \rho_s &= \alpha\rho + (1-\alpha)\rho_a \\ \mu_s &= \alpha\mu + (1-\alpha)\mu_a \end{aligned}. \tag{4}$$

Where ρ_s and μ_s is density and viscosity of the single continuum; ρ and ρ_a is density of the ink and the air, respectively; μ and μ_a is viscosity of the ink and the air, respectively.

Governing equations for FEF modeling include continuity equation, momentum equilibrium equation and phase fraction equation. Each equation of the two-phase incompressible laminar flow is written as follows [40]:

Continuity equation:

$$\nabla \cdot \mathbf{U} = 0. \tag{5}$$

Where $\mathbf{U}$ is velocity field of the fluid.

Momentum equilibrium equation:

$$\frac{\partial \rho_s \mathbf{U}}{\partial t} + \nabla \cdot (\rho_s \mathbf{U}\mathbf{U}) = -\nabla p + \nabla \cdot (\rho_s \mu_s \nabla \mathbf{U}) + \rho_s \mathbf{g} + \mathbf{F}_\sigma. \tag{6}$$

Where p is the pressure in the fluid; $\mathbf{g}$ is the gravitational acceleration vector; $\mathbf{F}_\sigma$ is surface tension. $\mathbf{F}_\sigma$ is defined as follows:

$$\mathbf{F}_\sigma = \sigma\kappa\nabla\alpha. \tag{7}$$

Where σ is the surface tension coefficient; κ is the surface curvature which is depended on the shape of FEF.

Phase fraction equation:

$$\frac{\partial \alpha}{\partial t} + \nabla \cdot (\alpha \mathbf{U}) + \nabla \cdot \left(\alpha(1-\alpha)\mathbf{U}_\mathbf{r}\right) = 0. \tag{8}$$

Where $\mathbf{U}_\mathbf{r}$ is velocity vector compressing two-phase free surface, which represents the velocity difference between two-phase fluids and can be calculated as follows:

$$\mathbf{U}_\mathbf{r} = \min\left(c|\mathbf{U}|, \max|\mathbf{U}|\right)\frac{\nabla\alpha}{|\nabla\alpha|}. \tag{9}$$

Where c is controllable compression factor and it is selected as c =1 in the numerical simulation.

Numerical simulation with VOF was implemented based on the solvers in OpenFOAM. The movement of the piston (B1) along axis direction was implemented using the motion solver, *velocityComponentLaplacian*. The governing equations for flow were solved based on the solver for two incompressible, isothermal immiscible fluids using VOF method with optional mesh motion and mesh topology changes including adaptive re-meshing, *interFoam*. *PIMPLE* algorithm, a combined algorithm of the pressure-implicit split-operator (*PISO*) and the semi-implicit method for pressure-linked equations (*SIMPLE*) algorithms, was chosen as the numerical algorithm for *interFoam* solver.

3.3. Evaluation indicators

Evaluation indicators of FEF include mean diameter and stability as continuous and tubular FEF with diameters close to the actual nozzle inner diameter is the basic requirement for a successful extrusion-based AM [41]. N measuring points were set along the filament length uniformly from nozzle bottom at fixed sampling intervals of 1 mm and diameter on each measuring point was measured as $d_i(i=1,2,...,N)$. Mean diameter and stability of FEF were expressed using average and standard deviation of $d_i(i=1,2,...,N)$, respectively.

4. Results and discussion

4.1. Material properties tests results

The density and surface tension coefficient of the prepared cellulose ink and the Nivea Crème were obtained by density and surface tension tests and the results were listed in Table 2.

Table 2 Results of density and surface tension coefficient for cellulose ink and Nivea Crème.

Ink	ρ (kg/m^3)	σ (mN/m)
Cellulose ink	1020	70
Nivea Crème	972	43

As shown in Fig. 3, μ_0, τ_0 were determined using the intersection point of two tangents in the diagram of shear stress ramp test data, one was stable platform line (red dotted line) in the plateau-region and one is the quickly-drop line (purple dotted line) in the viscosity-drop region. Abscissa and ordinate of the intersection point was μ_0 and τ_0, respectively. The results were listed in Table 3.

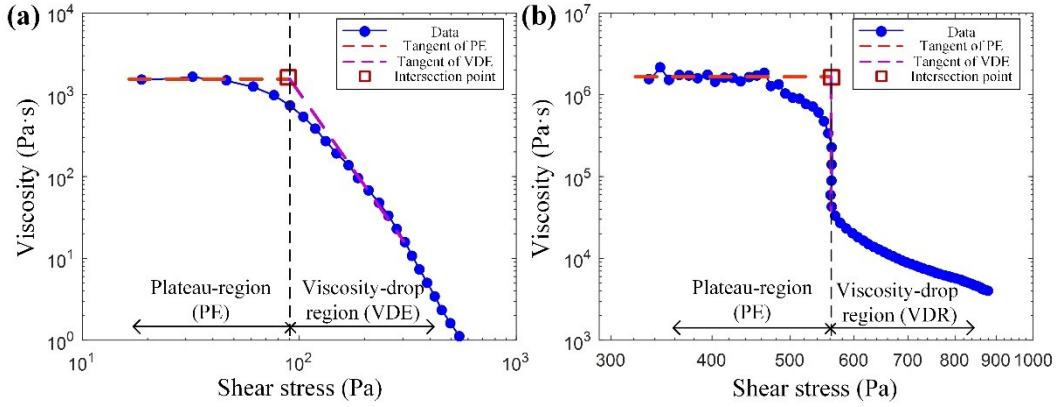

Fig. 3 Shear stress ramp data for (a) cellulose ink and (b) Nivea Crème.

Table 3 Results of yield stress and limiting dynamic viscosity for cellulose ink and Nivea Crème.

Ink	τ_0 (Pa)	μ_0 (Pa·s)
Cellulose ink	90	1650
Nivea Crème	563	1.58×10^6

As shown in Fig. 4, both cellulose ink and Nivea Crème demonstrated shear thinning behavior, characterized by the decrease in viscosity with increasing shear rate. Shear thinning parameters, K and n, were obtained by fitting Eq. (2) with the viscosity-shear rate data using data regression. The results were listed in Table 4. The coefficient of determination (R^2) and p-value of fitting results for cellulose ink was 0.9906 and 0.0000<0.05, and R^2 and p-value of fitting results for Nivea Crème was 0.9947 and 0.0000<0.05, verified the fitting results for the two inks.

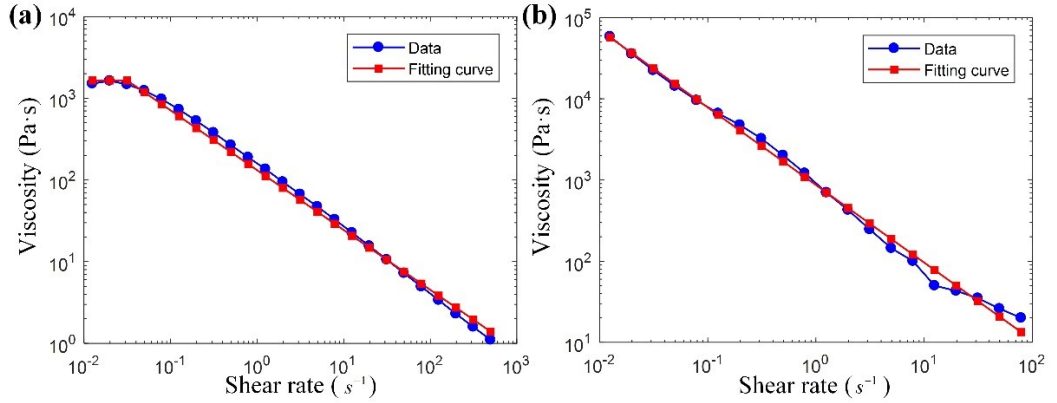

Fig. 4 Experimental data and fitting curve of shear rate sweep test for (a) cellulose ink and (b) Nivea Crème.

Table 4 Results of shear thinning parameters for cellulose ink and Nivea Crème.

Ink	K ($Pa\cdot s^n$)	n (Dimensionless)
Cellulose ink	132.72	0.268
Nivea Crème	867.02	0.045

4.2. Simulation results and experimental verification

In order to validate the proposed model, the prepared cellulose ink and Nivea Crème was

used as inks for FEF extrusion tests in a DIW 3D printer. As shown in Fig. 5a, a piston driven DIW 3D printer TM-081 (Tobeca Company, France) was used to extrude ink in the syringe into FEF in the air; and a camera (Canon LEGRIA HF R86 Noir, Canon Inc., Japan) was used to take photos of FEF. As shown in Fig. 5b, the extrusion tool in the DIW 3D printer was composed of a 30mL syringe (Braun Melsungen AG, Germany) and a precision engineered fluid dispensing nozzle (Nordson EFD, USA). Using the symbols in Fig. 1a, dimensions of extrusion tool were: D_s = 21.6 mm; D_n = 0.84 mm; L_n = 18 mm; initial L_s = 30 mm.

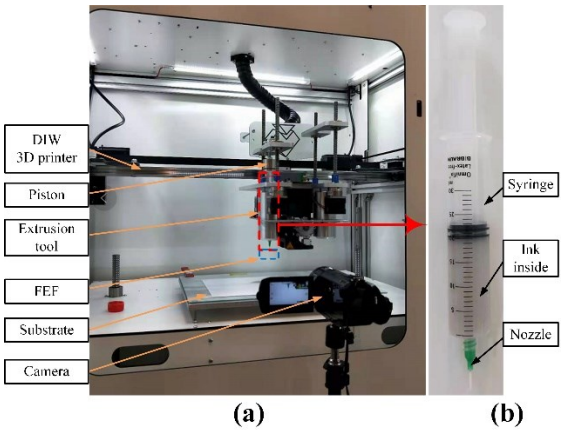

Fig. 5 Experimental validation setup for the proposed model: (a) producing FEF using DIW 3D printer and observing FEF using camera; (b) extrusion tool in the DIW 3D printer.

Disregarding ink compressibility, the mass conservation for the FEF producing process is expressed as:

$$v_p / v_e = \left(D_n / D_s\right)^2 , \tag{10}$$

Where v_p is the piston velocity, v_e is average velocity of FEF.

To verify the proposed model considering the universality for different process parameters, 3 levels of v_p were set by setting v_e from 5 mm/s to 15 mm/s at fixed intervals of 5 mm/s, which were on the printable range. The 3 levels setting for v_p was summarized in Table 5.

Table 5 Piston velocity setting in the experimental validation.

Levels	v_1	v_2	v_3
v_e (mm/s)	5	10	15
v_p (10^{-3} mm/s)	7.56	15.12	22.68

Simulation and experimental results for the cellulose ink and Nivea Crème under 3 levels of v_p were plotted in Fig. 6a and Fig. 6b, respectively. Here, all images were plotted using the same graphical scale in order to provide a direct comparison of simulation and experimental results. Modeling was verified by comparing simulation and experimental results for shape and diameter accuracy. For shape, all simulation results had continuous extruded profiles in accordance with experimental results by observing images in Fig. 6. Diameter accuracy described in Section 3.3 was used to verify the prediction accuracy of the model. Diameter

accuracy for the cellulose ink and Nivea Crème under 3 levels of v_p were summarized in Table 6, where the maximum error was 0.09 mm and the maximum relative error was 10.22%, verified the model had a high diameter accuracy. Thus, the model was verified both from shape and diameter accuracy.

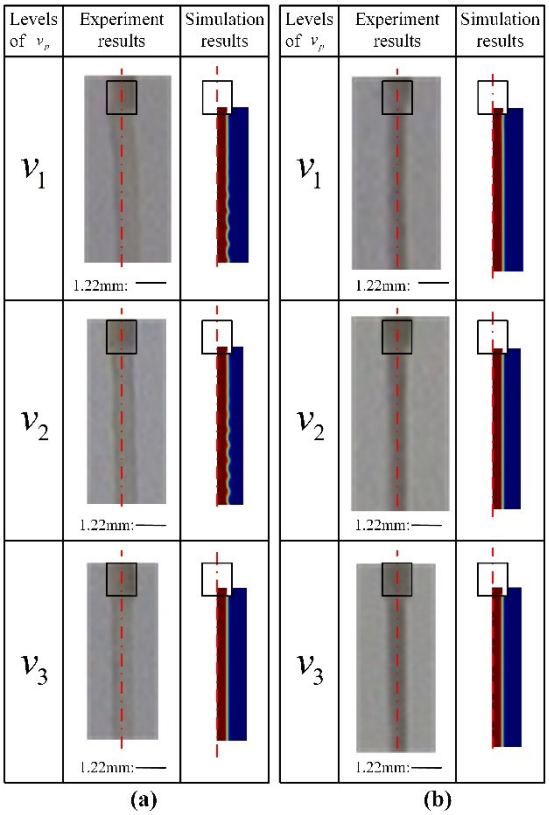

Fig. 6 Simulation and experimental results of FEF under 3 levels of piston velocities for: (a) cellulose ink; (b) Nivea Crème.

Table 6 Results of diameter accuracy of the proposed model for cellulose ink and Nivea Crème.

Ink	Diameter accuracy under 3 levels of v_p (mm)		
	v_1	v_2	v_3
Cellulose ink	0.07	0.09	0.06
Nivea Crème	0.02	0.08	0.04

4.3. Usages of the model

After experimental verification, the simulation model was used to evaluate the effect of the piston velocity on the FEF, characterize the ink printability and find suitable printable windows for process parameters with the two evaluation indicators. Firstly, v_p were set by setting v_e from 1 mm/s to 20 mm/s with Eq. (10) and used as input conditions in the proposed model. Then, the two evaluation indicators were used to evaluate FEF under different piston velocities based on the model. As shown in Fig. 7a, there was no continuous and stable FEF when setting of v_e was below 3 mm/s and 2 mm/s for the cellulose ink and Nivea Crème, respectively, as

piston velocity should be large enough to let FEF overcome yield stress and surface tension to produce continuous and stable filaments. The minimum setting of v_e to produce stable FEF for the cellulose ink was higher than that for Nivea Crème because surface tension coefficient of the cellulose ink was higher than that of Nivea Crème. When setting of v_e was higher than minimum setting of v_e to produce stable FEF, mean diameters of FEF decreased with increasing setting of v_e both for the cellulose ink and Nivea Crème. For the cellulose ink, mean diameters of FEF got closer to the nozzle inner diameter as setting of v_e increased ranging from 1 mm/s to 20 mm/s. For Nivea Crème, mean diameters of FEF got closer to the nozzle inner diameter as setting of v_e increased ranging from 1 mm/s to 10 mm/s and was equal to nozzle inner diameter when setting of v_e was 10 mm/s. Then, it moved further away from the nozzle inner diameter as the setting of v_e was higher than 10 mm/s. As shown in Fig. 7b, stability decreased firstly and then increased as setting of v_e increased ranging from 1 mm/s to 20 mm/s both for the cellulose ink and Nivea Crème. From Fig. 7, it is concluded that the printability of Nivea Crème was better than the cellulose ink as mean diameter got closer to the nozzle inner diameter and stability was much smaller for Nivea Crème compared with the cellulose ink. Meanwhile, considering the requirement that FEF should have mean diameter close to nozzle inner diameter and good stability, printable window of setting of v_e for FEF was summarized from Fig. 7: 15mm/s-20 mm/s for the cellulose ink; 5 mm/s-15 mm/s for Nivea Crème.

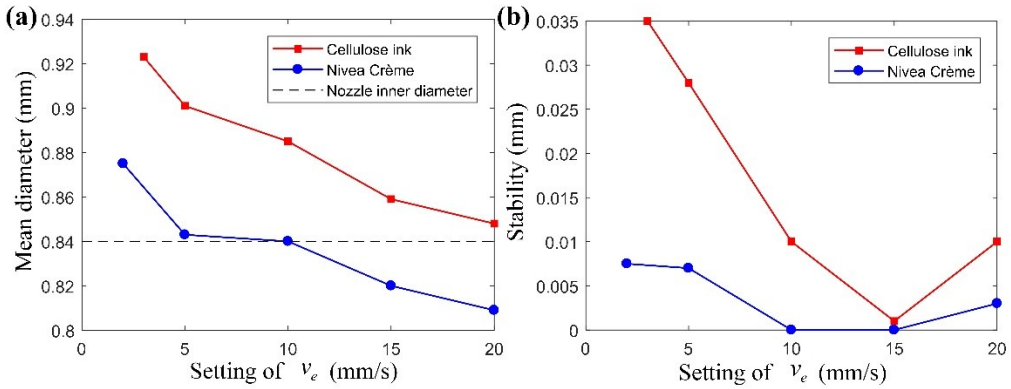

Fig. 7 Evaluation of the FEF for cellulose ink and Nivea Crème using the proposed two evaluation indicators as: (a) mean diameter; (b) stability.

5. Conclusions

In this study, a model of FEF was established with numerical simulation method and then the FEF was evaluated based on this model. First, ink properties were determined by properties tests. Then, model of FEF was established using numerical simulation method and two evaluation indicators, mean diameter and stability, were proposed to evaluate the FEF. Finally, two inks, a cellulose ink and a Nivea Crème, were used to verify the method. The established model was verified as the shape in simulation was in accordance with experimental results and diameter accuracy was better than 0.09 mm. After experimental verification, the model and evaluation indicators were used to deal with these three questions in DIW as:

(1) Analyze effect of the piston velocity on FEF: there was a minimum piston velocity, 3 mm/s for the cellulose ink and 2 mm/s for Nivea Crème for setting of v_e, to produce continuous and stable FEF; mean diameters of FEF decreased with increasing piston velocity. Stability

decreased firstly and then increased as piston velocity increased,

(2) Characterize the ink printability: the printability of Nivea Crème was better than the cellulose ink as mean diameter got closer to the nozzle inner diameter and stability was much smaller for Nivea Crème compared with the cellulose ink,

(3) Find suitable printable windows for process parameters: printable window of setting of v_e was 15mm/s-20 mm/s for the cellulose ink and 5 mm/s-15 mm/s for Nivea Crème.

Future work could establish a simulation model of the filaments deposited on the substrate considering the ink properties and process parameters. The printing quality could then be improved by using the established simulation model in order to extend the FEF contribution in this study to deposited filaments.

References

[1] J. Cesarano, R. Segalman, P. Calvert, ROBOCASTING PROVIDES MOLDLESS FABRICATION FROM SLURRY DEPOSITION, Ceramic industry, 148 (1998).

[2] J. Cesarano, P. Calvert, FREEFORMING OBJECTS WITH LOW BINDER SLURRY, United States, 2000.

[3] N. Hossain, M.A. Chowdhury, M.B.A. Shuvho, M.A. Kashem, M. Kchaou, 3D-Printed Objects for Multipurpose Applications, Journal of Materials Engineering and Performance, (2021).

[4] P. Kumar, D.K. Rajak, M. Abubakar, S.G.M. Ali, M. Hussain, 3D Printing Technology for Biomedical Practice: A Review, Journal of Materials Engineering and Performance, (2021).

[5] M. Kim, J.-W. Choi, Rubber ink formulations with high solid content for direct-ink write process, Additive Manufacturing, 44 (2021) 102023.

[6] D.F.D. Campos, M.A. Philip, S. Gürzing, C. Melcher, Y.Y. Lin, J. Schöneberg, A. Blaeser, B. Theek, H. Fischer, M. Betsch, Synchronized Dual Bioprinting of Bioinks and Biomaterial Inks as a Translational Strategy for Cartilage Tissue Engineering, 3D Printing and Additive Manufacturing, 6 (2019) 63-71.

[7] T. Kim, C. Bao, M. Hausmann, G. Siqueira, T. Zimmermann, W.S. Kim, 3D Printed Disposable Wireless Ion Sensors with Biocompatible Cellulose Composites, Advanced Electronic Materials, 5 (2019) 1800778.

[8] Z. Ye, C. Chu, D. Zhang, S. Ma, J. Guo, Y. Cheng, G. Xu, Z. Li, A. Sun, Study on 3D-Direct Ink Writing based on adding silica submicron-particles to improve the rheological properties of alumina ceramic ink, Materials Today Communications, 28 (2021) 102534.

[9] M.C. Mulakkal, R.S. Trask, V.P. Ting, A.M. Seddon, Responsive cellulose-hydrogel composite ink for 4D printing, Materials & Design, 160 (2018) 108-118.

[10] Q. Wang, J. Sun, Q. Yao, C. Ji, J. Liu, Q. Zhu, 3D printing with cellulose materials, Cellulose, 25 (2018) 4275-4301.

[11] C. Thibaut, A. Denneulin, S. Rolland du Roscoat, D. Beneventi, L. Orgéas, D. Chaussy, A fibrous cellulose paste formulation to manufacture structural parts using 3D printing by extrusion, Carbohydrate Polymers, 212 (2019) 119-128.

[12] M. Lille, A. Nurmela, E. Nordlund, S. Metsä-Kortelainen, N. Sozer, Applicability of protein and fiber-rich food materials in extrusion-based 3D printing, Journal of Food Engineering, 220 (2018) 20-27.

[13] L.A. Vergara, H.A. Colorado, Additive manufacturing of Portland cement pastes with additions of kaolin, superplastificant and calcium carbonate, Construction and Building Materials, 248 (2020)

118669.
[14] A. Shahzad, I. Lazoglu, Direct ink writing (DIW) of structural and functional ceramics: Recent achievements and future challenges, Composites Part B: Engineering, 225 (2021) 109249.
[15] P.T. Smith, A. Basu, A. Saha, A. Nelson, Chemical modification and printability of shear-thinning hydrogel inks for direct-write 3D printing, Polymer, 152 (2018) 42-50.
[16] L. Ouyang, R. Yao, Y. Zhao, W. Sun, Effect of bioink properties on printability and cell viability for 3D bioplotting of embryonic stem cells, Biofabrication, 8 (2016) 035020.
[17] N. Paxton, W. Smolan, T. Böck, F. Melchels, J. Groll, T. Jungst, Proposal to assess printability of bioinks for extrusion-based bioprinting and evaluation of rheological properties governing bioprintability, Biofabrication, 9 (2017) 044107.
[18] J.L. Dávila, M.A. d'Ávila, Rheological evaluation of Laponite/alginate inks for 3D extrusion-based printing, The International Journal of Advanced Manufacturing Technology, 101 (2019) 675-686.
[19] Y. He, F. Yang, H. Zhao, Q. Gao, B. Xia, J. Fu, Research on the printability of hydrogels in 3D bioprinting, Scientific Reports, 6 (2016) 29977.
[20] G. Percoco, L. Arleo, G. Stano, F. Bottiglione, Analytical model to predict the extrusion force as a function of the layer height, in extrusion based 3D printing, Additive Manufacturing, 38 (2021) 101791.
[21] N. Ashrafi, S. Nazarian, N.A. Meisel, J.P. Duarte, Experimental prediction of material deformation in large-scale additive manufacturing of concrete, Additive Manufacturing, 37 (2021) 101656.
[22] N. Roussel, J. Spangenberg, J. Wallevik, R. Wolfs, Numerical simulations of concrete processing: From standard formative casting to additive manufacturing, Cement and Concrete Research, 135 (2020) 106075.
[23] F. Liravi, R. Darleux, E. Toyserkani, Additive manufacturing of 3D structures with non-Newtonian highly viscous fluids: Finite element modeling and experimental validation, Additive Manufacturing, 13 (2017) 113-123.
[24] J. Göhl, K. Markstedt, A. Mark, K. Håkansson, P. Gatenholm, F. Edelvik, Simulations of 3D bioprinting: predicting bioprintability of nanofibrillar inks, Biofabrication, 10 (2018) 034105.
[25] R. Comminal, W.R. Leal da Silva, T.J. Andersen, H. Stang, J. Spangenberg, Modelling of 3D concrete printing based on computational fluid dynamics, Cement and Concrete Research, 138 (2020) 106256.
[26] R. Suntornnond, E.Y. Tan, J. An, C.K. Chua, A Mathematical Model on the Resolution of Extrusion Bioprinting for the Development of New Bioinks, Materials, 9 (2016).
[27] A. Schwab, R. Levato, M. D'Este, S. Piluso, D. Eglin, J. Malda, Printability and Shape Fidelity of Bioinks in 3D Bioprinting, Chemical Reviews, 120 (2020) 11028-11055.
[28] C. Demitri, R. Del Sole, F. Scalera, A. Sannino, G. Vasapollo, A. Maffezzoli, L. Ambrosio, L. Nicolais, Novel superabsorbent cellulose-based hydrogels crosslinked with citric acid, Journal of Applied Polymer Science, 110 (2008) 2453-2460.
[29] T.V.C. McOscar, W.M. Gramlich, Hydrogels from norbornene-functionalized carboxymethyl cellulose using a UV-initiated thiol-ene click reaction, Cellulose, 25 (2018) 6531-6545.
[30] Y. Tu, J.A. Arrieta-Escobar, A. Hassan, U.K.u. Zaman, A. Siadat, G. Yang, Optimizing Process Parameters of Direct Ink Writing for Dimensional Accuracy of Printed Layers, 3D Printing and Additive Manufacturing, (2021).

[31] M.H. Kim, Y.W. Lee, W.-K. Jung, J. Oh, S.Y. Nam, Enhanced rheological behaviors of alginate hydrogels with carrageenan for extrusion-based bioprinting, Journal of the Mechanical Behavior of Biomedical Materials, 98 (2019) 187-194.
[32] F. Koch, K. Tröndle, G. Finkenzeller, R. Zengerle, S. Zimmermann, P. Koltay, Generic method of printing window adjustment for extrusion-based 3D-bioprinting to maintain high viability of mesenchymal stem cells in an alginate-gelatin hydrogel, Bioprinting, (2020) e00094.
[33] C. Busse, I. Tsivilskiy, J. Hildebrand, J.P. Bergmann, Numerical modeling of an inductively coupled plasma torch using OpenFOAM, Computers & Fluids, 216 (2021) 104807.
[34] W. Ge, M.F. Modest, R. Marquez, Two-dimensional axisymmetric formulation of high order spherical harmonics methods for radiative heat transfer, Journal of Quantitative Spectroscopy and Radiative Transfer, 156 (2015) 58-66.
[35] N. Scapin, P. Costa, L. Brandt, A volume-of-fluid method for interface-resolved simulations of phase-changing two-fluid flows, Journal of Computational Physics, 407 (2020) 109251.
[36] M.R. Hashemi, P.B. Ryzhakov, R. Rossi, An enriched finite element/level-set method for simulating two-phase incompressible fluid flows with surface tension, Computer Methods in Applied Mechanics and Engineering, 370 (2020) 113277.
[37] J. Yang, J. Kim, A phase-field method for two-phase fluid flow in arbitrary domains, Computers & Mathematics with Applications, 79 (2020) 1857-1874.
[38] L. Zheng, S. Zheng, Q. Zhai, Reduction-consistent axisymmetric lattice Boltzmann equation method for N-phase fluids, Computers & Fluids, 218 (2021) 104857.
[39] M. Li, I.A. Bolotnov, The evaporation and condensation model with interface tracking, International Journal of Heat and Mass Transfer, 150 (2020) 119256.
[40] M.R.P. de Sousa, H.S. Santana, O.P. Taranto, Modeling and simulation using OpenFOAM of biodiesel synthesis in structured microreactor, International Journal of Multiphase Flow, 132 (2020) 103435.
[41] P. Geng, J. Zhao, W. Wu, W. Ye, Y. Wang, S. Wang, S. Zhang, Effects of extrusion speed and printing speed on the 3D printing stability of extruded PEEK filament, Journal of Manufacturing Processes, 37 (2019) 266-273.